Bending of a Stented Atherosclerotic Artery

Henry C. Wong[*,1], Kevin N. Cho and William C. Tang[2]
[1,2]Department of Biomedical Engineering, University of California, Irvine
*Corresponding author: 3120 Natural Sciences II, UC Irvine, Irvine, CA 92697-2715, hcwong@uci.edu

Abstract: Atherosclerosis causes the deposition of plaque on the inner walls of arteries, which leads to restricted blood flow. Using the balloon angioplasty procedure, stents can be inserted and expanded in the atherosclerotic artery. The current stent designs are not ideal for use in arteries that undergo large bending deformations. We investigated a novel segmented stent design for use in this class of arteries. In our study, we used COMSOL Multiphysics to simulate the bending of an atherosclerotic artery with (i) two 6-mm stent segments and (ii) one 48-mm stent. Our results show that lower stent stresses were obtained as the spacing between the stents was increased. Also, the maximum stresses in the 48-mm stent were greater than those in the 6-mm segments as the artery was bent. This specialized stent design could prove to be optimal for use in arteries that undergo significant bending, such as the superficial femoral artery.

Keywords: Atherosclerosis, large bending deformation, stent segments, numerical simulation.

1. Introduction

Atherosclerosis is one of the leading causes of death in the United States [1]. It is a complex disease that is usually characterized by the deposition of plaque on the inner walls of arteries, which leads to restricted blood flow. The early stage of atherosclerosis involves the thickening of the intimal layer of the artery. Subsequently, the deposition of lipid and fibrous tissue can occur. As the disease progresses, the plaque becomes more dense as more fibrous tissue and calcium get deposited. The locations that the plaque develops are usually where turbulent flow is high, such as at arterial bifurcations [2].

One of the most common treatments is the balloon angioplasty procedure in which a stent is inserted and expanded using a balloon in order to open up the occluded artery to increase blood flow. Many computational studies have been done to predict the deformation and stresses involved in such a procedure. Three different methods have been used to model the expansion of the stent: pressure applied on the internal surface of the stent, displacement applied on a rigid cylindrical surface, and inflation of a balloon in contact with the stent [3]. For instance, F. Gervaso, *et al*. investigated several methods of stent expansion, including when the stent was confined within a coronary artery and when it was allowed to freely expand [4]. The effects of the balloon structure on the free expansion of a stent were also investigated by M. De Beule, *et al*. Their group compared the expansion of the stent for the following cases: applied pressure on the internal surface of a trifolded balloon, applied radial displacement on a cylindrical balloon, and applied internal pressure with no balloon [5]. From these examples it is evident that extensive research has been conducted on stent expansion. However, fewer computational studies have been done on stented atherosclerotic arteries that undergo significant bending.

The stents that are currently being used by surgeons are not ideal for use in arteries that undergo large bending, such as the superficial femoral artery (SFA). The bending of the artery may lead to severe deformation of the stent itself and crimping of the stent. Furthermore, due to cyclic loading and high stresses, yielding of the stent and severe damage to the arterial wall may also occur during this process. The objective of our study was to determine the effects of various stent configurations on the bending of an atherosclerotic artery. More specifically, we wanted to compare the usage of short stent segments with a full-length stent. We ran simulations using the commercial software COMSOL Multiphysics version 3.5a.

2. Materials

2.1. Model Geometry

The artery was modeled as a hollow cylinder with an inner radius of 3 mm, a thickness of 0.7

mm, and a longitudinal length of 8 cm. The plaque was modeled with an inner radius of 2 mm, a thickness of 1 mm, and a length of 8 cm. We used a full-length stent (with a length of 48 mm) and stent segments (each with a length of 6 mm) in our simulations. For each of the stents, the inner radius was 1.8 mm and the thickness was 0.2 mm. The longitudinal axis corresponded to the z-axis, and the median planes of the artery and plaque were located at $z = 0$. Two sets of boundary conditions were used in the simulations. For the first set, the artery and plaque were fixed at the $z = 0$ plane, and a transverse displacement in the y-direction was applied to the ends of the artery at $z = \pm 4$ cm planes. For the second set of boundary conditions, a single point on the artery was fixed at $z = 0$, a symmetry boundary condition was applied on the $z = 0$ plane, and transverse displacements were applied at single points at the ends of the artery at $z = \pm 4$ cm. For both sets of boundary conditions, the model was symmetrical with respect to the $z = 0$ and $x = 0$ planes. Due to this symmetry in the bending configuration, one-fourth of the artery-plaque-stent model was created in COMSOL. Thus, the regions where $x > 0$ and $z > 0$ were explicitly modeled.

For our simulations, the artery, plaque, and stent were assumed to be a composite geometry in which COMSOL treated the system as one solid object with 3 different sub-domains. Thus, the software provided continuity for the displacement and provided a conforming mesh at the artery-plaque and plaque-stent interfaces [6]. The three sub-domains were still preserved, allowing us to assign different material properties for the artery, plaque, and stent regions. In our simulations we used the displacement-controlled approach with Lagrangian linear elements. The maximum element sizes used in the artery and plaque sub-domains were chosen as 0.6 mm, and 0.5 mm, respectively. A finer mesh was used in the region of contact between the stent and the plaque. The maximum element size on this region was chosen to be 0.25 mm, and that within the stent sub-domain was also chosen to be 0.25 mm. The number of elements for the system was approximately 125,000 when the stent segment was used and 225,000 when the full-length stent was used. The numbers of degrees of freedom were typically greater than 560,000 and 900,000 when the single and full-length stent were used, respectively.

2.2. Material Properties

The stress-strain relationships of most biological tissues are nonlinear. Many experiments have been done to characterize the mechanical properties of arteries. In computational studies, isotropic hyperelastic strain energy functions are often used for the artery and plaque, such as those used by I. Pericevic, *et al*. [7]. To simplify the numerical analysis, the artery and plaque were modeled using a hyperelastic, neo-Hookean strain energy function:

$$W = \frac{\mu}{2}(\bar{I}_1 - 3) + \frac{K}{2}(J-1)^2, \qquad (1)$$

where

$$\bar{I}_1 = \frac{B_{kk}}{J^{2/3}} \qquad (2)$$

is the first modified invariant of the left Cauchy-Green deformation tensor B_{ij}. Also,

$$B_{ij} = F_{ik}F_{jk}, \qquad (3)$$

$$J = \det \mathbf{F}, \qquad (4)$$

$$F_{ij} = \delta_{ij} + \frac{\partial u_i}{\partial X_j}, \qquad (5)$$

where F_{ij} is the deformation gradient tensor, u_i refers to the displacement components, X_i refers to the undeformed coordinates and δ_{ij} is the Kronecker delta [8]. For small deformations, μ and K are equivalent to the shear and bulk modulus, respectively, for a linearly elastic material. For the artery, the initial shear modulus was 6 MPa [9], whereas for the plaque, $\mu = 6$ kPa was used in the numerical simulations. Most biological tissues are nearly incompressible. Thus, it was assumed that $K = 20\mu$ [9], which corresponded to a Poisson's ratio of about 0.475 for small deformations since

$$\nu = \frac{3K - 2\mu}{2(3K + \mu)}. \qquad (6)$$

Because $E = 2\ \mu(1+\nu)$ [8], the initial shear modulus for the plaque ($\mu = 6$ kPa) corresponded to an initial Young's modulus (E) that was 1/1000 that of the arterial wall. The stent was made of nitinol, a superelastic shape memory alloy (SMA). A notable feature of the stress-strain curve for nitinol is the closed hysteresis loop that can be observed when the material is

loaded to a large enough strain and then unloaded. This is a result of the reversible phase transformation that occurs between the austenite and martensite crystalline structures [10]. Thus, the mechanical and thermal properties of nitinol are coupled. The transformation from austenite to martensite is exothermic whereas the opposite is true for the reverse transformation [11]. If nitinol is strained up to 7-8%, it is able to return to its original configuration when the load is removed. For small strains, it behaves like a linearly elastic material. We used the material model described by W. Wu, *et al*., where nitinol behaved like a linearly elastic isotropic solid if it was loaded up to 346 MPa. In our simulations, since the stresses were significantly lower, we used 60 GPa for the Young's modulus and 0.33 for the Poisson's ratio [12].

3. Numerical Simulation

We used COMSOL Multiphysics Structural Mechanics, Solid Stress-Strain module to perform static, large deformation analyses. As mentioned earlier, we conducted our simulations for two sets of boundary conditions where one-fourth of the stented artery-plaque model was explicitly modeled. In the first set of boundary conditions, the median planes (z = 0) of the artery and plaque were fixed and the transverse displacement was applied on the surface at the end of the artery (z = 4 cm). In the second set, the artery was fixed at a single point at z = 0, a symmetry boundary condition was applied on the z = 0 plane, and the displacement was applied at a single point at z = 4. This displacement-controlled approach was taken in order to ensure the stability of the simulations. The simulations were conducted for a stent segment located at z = 1, 1.5, 2, and 2.5 cm. Because of symmetry, these corresponded to 2 stent segments with spacing of $2z$ = 2, 3, 4, and 5 cm, respectively. For comparison purposes, simulations were also done for the 48 mm full-length stent where the second set of boundary conditions was used.

For the simulations with the segmented stent design the parametric solver was used to incrementally increase the applied transverse displacement in 1 mm steps starting from 1 mm. For each applied displacement the nonlinear solver, based on a damped Newton's method [6], was used to solve for the deformation. The maximum number of iterations permitted for each parameter step was 200. Obtaining a converged solution for the first step was the most difficult, often requiring more than 100 iterations. However, subsequent steps converged in a few iterations. This was because the parametric solver was used, which allowed the converged solution from the previous step to be used as a starting point for the computation of the next step.

In our simulations, we neglected the radial expansion of the stent and assumed that the stent was in contact with the plaque in the initial configuration. We assumed that this was the zero-stress state of the stent, and consequently, the stresses induced within the stent were a result of the bending of the atherosclerotic artery and its interactions with the stent. Our goal was to optimize the functionality of a stent based upon various design parameters which included bending angles, stresses, and the degree of crimping. With a segmented stent design, we hypothesized that as the artery bended, each stent section should not undergo a large amount of deformation. Therefore, the stent should not experience significant crimping or high mechanical stresses.

4. Results and Discussion

We first obtained results for the bending of the atherosclerotic artery with two stents, each with a length of 6 mm. This entailed running simulations for the two sets of boundary conditions previously mentioned in the "Numerical Simulation" section. The second set allowed greater amount of movement at the median planes of the artery and plaque. Figure 1 shows typical deformed shapes for both sets of boundary conditions. The applied transverse displacement was 13 mm and the distance between the two stents was 3 cm. For visualization purposes, the ranges for the von Mises stress were restricted.

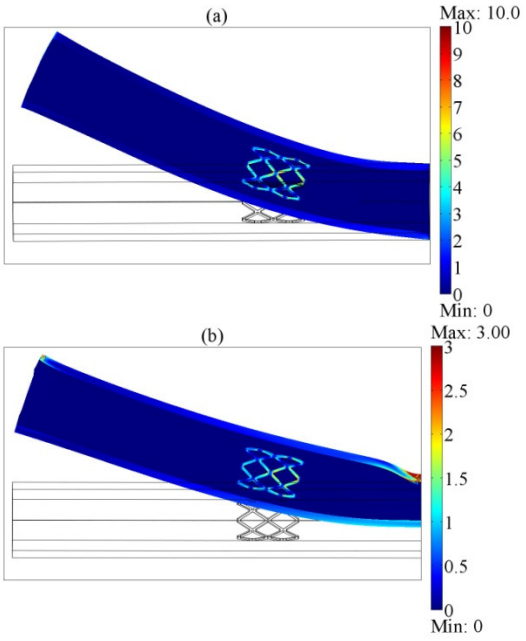

Figure 1. Plots of deformation for an applied transverse displacement of 13 mm for stents segment with a spacing of 3 cm. Colors indicate intensity of von Mises stresses (in MPa). (a) First set of boundary conditions. (b) Second set of boundary conditions.

Figure 2 shows a close-up plot of the von Mises stress (in MPa) for an applied displacement of 13 mm and for stent spacing of 3 cm. The second set of boundary conditions was used. For this case, the maximum von Mises stress was 4.05 MPa while the average was 0.55 MPa. The computed stent stress distribution was similar when the first set of boundary conditions was used, though the maximum and average were 13.58 and 1.94 MPa, respectively.

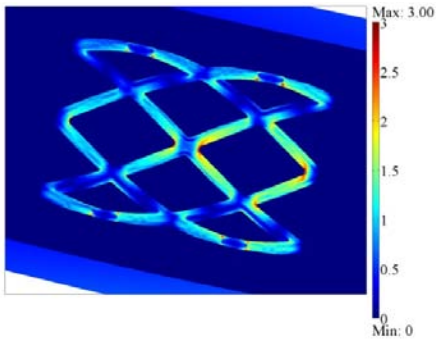

Figure 2. Von Mises stress distribution (in MPa) for second set of boundary conditions. The applied displacement was 13 mm and the stent spacing was 3 cm.

Figure 3 shows the plots of the maximum von Mises stresses in the stent segments as a function of the applied transverse displacement on the ends of the artery. The first set of boundary conditions was used for (a) whereas the second set was used for (b). Since the stresses in the stent were much lower than 346 MPa, the linearly elastic assumption used for nitinol was valid [12]. The average von Mises stresses were also computed, i.e.

$$\bar{\sigma}_{VM} = \frac{1}{|\Omega|}\int_{\Omega} \sigma_{VM}\, dV, \qquad (7)$$

where σ_{VM} is the von Mises stress distribution and Ω refers to the sub-domain of the stent. The maximum and average stresses followed the same trend, but the average was generally more than 5 times lower.

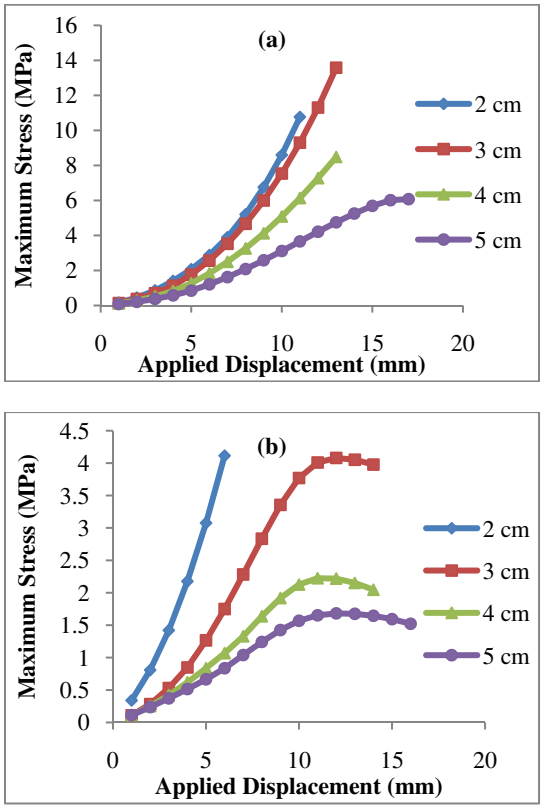

Figure 3. Plots of the maximum von Mises stress in the 2 stent segments as a function of the applied transverse displacement on the end of the artery for different stent spacings (2, 3, 4, 5 cm). (a) First set of boundary conditions were used. (b) Second set of boundary conditions were used.

In Fig. 3a, as the applied displacement was increased, the maximum stresses in the stent also increased. In particular, the stents with a spacing of 5 cm showed a more gradual increase in the stresses as the displacement was increased. On the other hand, for stent spacings of 3, 4, and 5 cm in Fig. 3b, the stresses showed an eventual decline as the applied displacement was increased. Note that the stent stresses were generally lower when the second set of boundary conditions was used rather than the first. This was due to the greater amount of movement allowed at the median planes of the artery and plaque in the second set. For all of the cases, the greater the spacing between the 2 stent segments (or the further the stents were located from the median plane), the lower the maximum stresses. A greater amount of rigid body movement was observed in the region of the artery and plaque that was further from the median plane. However, that region deformed to a lesser extent. On the other hand, near the median plane of the artery and plaque, a greater amount of deformation was observed. The interactions between the plaque and the stents resulted in larger deformations for stents situated closer to the median plane. Consequently, the mechanical stresses in the stent were higher.

For the simulations with the 48-mm stent, we applied displacements of 0.1, 0.25, and 0.5 mm at the ends of the artery. The reason why we applied smaller displacements was due in part to the mechanical model of nitinol that we used. Since we assumed linearly elastic behavior with a Young's modulus of 60 GPa and a Poisson's ratio of 0.33, larger applied displacements on the artery ends would have resulted in significantly larger stent strains and stresses. If the stresses exceeded 346 MPa, where the linearly elastic behavior would have been violated [12], then the predicted stent stresses would not have been realistic. Figure 4 shows the von Mises stress distribution (in MPa) in a region of the 48-mm stent for an applied displacement of 0.5 mm on the artery ends. The range was restricted from 0.3 to 100 MPa for visualization purposes. As shown in the figure, the stresses were concentrated in small areas. For applied displacements of 0.1, 0.25, and 0.5 mm, the maximum stresses were 48.66, 121.20, and 244.44 MPa, respectively. These stresses were significantly higher than those computed in the 6-mm stent segments. In particular, when a 1-mm displacement was applied on the ends of the artery, the maximum stress was 0.16 MPa when the first set of boundary conditions was used and 0.34 MPa when the second set was used. Also, the highest stress that we computed in the stent segments was 13.58 MPa, which occurred when the segments were separated by 3 cm and a 13-mm displacement was applied. This shows that using two 6-mm stent segments instead of the 48-mm stent greatly reduced the stent stresses induced by the bending of the artery.

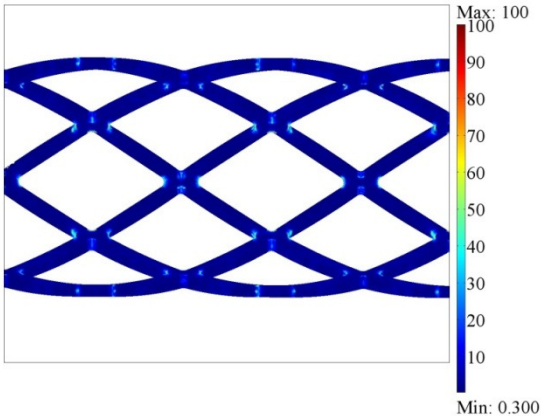

Figure 4. Von Mises stress distribution (in MPa) in a region of the full-length stent for an applied transverse displacement of 0.5 mm.

4. Conclusion

We have simulated the bending of an atherosclerotic artery with two 6-mm stent segments and with a 48-mm stent. The locations of the stents were varied but were always symmetrical with respect to the median plane of the artery. The computed results show that lower maximum and average von Mises stresses in the stent segments were obtained as the spacing between the segments was increased. In general, as the applied displacement was increased, higher stresses were observed in the stent segments. The two sets of boundary conditions that were used also affected the deformation of the artery and the stresses in the stent segments. More investigation will be needed to ascertain which set is more biologically realistic. It was also determined that the full-length stent experienced significantly higher stresses than the two 6-mm segments as the atherosclerotic artery was bent. In the future, more stent segments

with various longitudinal lengths should be included to further investigate the segmented stent design. For our current design, simulations can be done on the bending of the artery when three to seven 6-mm stent segments are used. Also, because the mechanical properties of the plaque are highly variable and the initial shear modulus (for a neo-Hookean model) could range from 0.1 to 60 kPa [13, 14, 15], the effects of the plaque stiffness on the stent stresses should be investigated. Lastly, radial expansion of the stent should be considered to make more realistic predictions of the stresses induced in the stents.

In our current work, we have showed that a segmented stent design provides lower stresses than a full-length stent. This specialized design could prove more useful in arteries that undergo large bending deformations. More experimental and simulation work will lead to an optimal segmented stent configuration for use in this class of arteries.

References

1. M.G. Bourassa, J.C. Tardif, *Antioxidants and Cardiovascular Disease*. Springer Science+Business Media, New York, NY (2006).
2. J.P. O'Leary, A. Tabuenca, *The Physiologic Basis of Surgery*. Lippincott Williams and Wilkins, Philadelphia, PA (2008).
3. C. Capelli, F. Gervaso, L. Petrini, G. Dubini, F. Migliavacca, "Assessment of tissue prolapse after balloon-expandable stenting: influence of stent cell geometry," *Medical Engineering and Physics,* **31**, 441-447 (2009).
4. F. Gervaso, C. Capelli, L. Petrini, S. Lattanzio, L. Di Virgilio, F. Migliavacca, "On the effects of different strategies in modeling balloon-expandable stenting by means of finite element method," *Journal of Biomechanics,* **41**, 1206-1212 (2008).
5. M. De Beule, P. Mortier, S.G. Carlier, B. Verhegghe, R. Van Impe, P. Verdonck, "Realistic finite element-based stent design: the impact of balloon folding," *Journal of Biomechanics*, **41**, 383-389 (2008).
6. *Structural Mechanics Module: User's Guide*, COMSOL Multiphysics v. 3.5a (2008).
7. I. Pericevic, C. Lally, D. Toner, D.J. Kelly, "The influence of plaque composition on underlying arterial wall stress during stent expansion: the case for lesion-specific stents," *Medical Engineering and Physics,* **31**, 428-433 (2009).
8. A.F. Bower, *Applied Mechanics of Solids*. CRC Press (2009).
9. *Structural Mechanics Module: Model Library*, COMSOL Multiphysics v. 3.5a (2008).
10. J.H. Kim, T.J. Kang, W.R. Yu, "Mechanical modeling of self-expandable stent fabricated using braiding technology," *Journal of Biomechanics,* **41**, 3202-3212 (2008).
11. F. Thiebaud, C. Lexcellent, M. Collet, E. Foltete, "Implementation of a model taking into account the asymmetry between tension and compression, the temperature effects in a finite element code for shape memory alloys structures calculations," *Computational Materials Science,* **41**, 208-221 (2007).
12. W. Wu, M. Qi, X.P. Liu, D.Z. Yang, W.Q. Wang, "Delivery and release of nitinol stent in carotid artery and their interactions: A finite element analysis," *Journal of Biomechanics,* **40**, 3034-3040 (2007).
13. D.E. Kiousis, T.C. Gasser, G.A. Holzapfel, "A numerical model to study the interaction of vascular stents with human atherosclerotic lesions," *Annals of Biomedical Engineering,* **35**, 1857-1869 (2007).
14. S.A. Kock, J.V. Nygaard, N. Eldrup, E.T. Frund, A. Klaerke, W.P. Paaske, E. Falk, W.Y. Kim, "Mechanical stresses in carotid plaques using MRI-based fluid-structure interaction models," *Journal of Biomechanics,* **41**, 1651-1658 (2008).
15. D. Tang, C. Yang, J. Zheng, P.K. Woodard, G.A. Sicard, J.E. Saffitz, C. Yuan, "3D MRI-based multicomponent FSI models for atherosclerotic plaques," *Annals of Biomedical Engineering,* **32**, 947-960 (2004).

Acknowledgements

The authors would like to thank Robert Giasolli from Innovasc for extensive discussions on his original concept of the segmented stent design and partial initial funding for the work. We also recognize Jim Greene for his contributions in the initial stages of this project.